A correction method for large deflections of cantilever beams with modal approach

Ozan Gözcü[1], Emre Barlas[2], and Suguang Dou[1]

[1]DTU Wind Energy, Technical University of Denmark (DTU), Frederiksborgvej 399, 4000 Roskilde, Denmark
[2]Ørsted, Nesa Allè 1, 2820 Gentofte

Correspondence to: Ozan Gözcü(ozgo@dtu.dk)

Abstract. Modal based reduced order models are preferred for modelling structures due to their computational efficiency in engineering problems. One of the important limitations of the classic modal approaches is that they are geometrically linear. This study proposes a fast correction method to account for geometric non-linearities which stem from large deflections in cantilever beams. The method relies on pre-computed correction terms and thus adds negligibly small extra computational efforts during the time domain response analyses. The accuracy of the method is examined on a straight beam and IEA 15 MW wind turbine blade model. The results show that the proposed method increases the accuracy of modal approach significantly in secondary deflections due to nonlinearities such as axial and torsional motions for the two studied cases.

Keywords : Geometric nonlinearity, modal reduction, modal derivatives, expansion modes, IEA 15MW turbine

1 Introduction

Reduced order models (ROMs) based on modal approach are used in many structural engineering problems such as wind turbine blades (Hansen, 2015), aircraft wings (Bisplinghoff et al., 2013), space crafts (Marshall and Pellegrino, 2021) due to their computational efficiency and reasonable accuracy. These ROMs are based on the small deflection assumption, in other words they use constant stiffness, mass and damping matrices which are not updated by deflections unlike nonlinear models. Hence, the accuracy of modal based ROMs reduces as deflections increase and their errors become significant for applications with large deflections such as long and flexible wind turbine blades or aircraft wings. Moreover, the error in structural response amplifies the error in aeroelastic response and load analysis due to the coupled nature of the problem.

The large deflection effects on aeroelastic stability and loads for wind turbine blades (Kallesøe, 2011; Beardsell et al., 2016; Collier and Sanz, 2016; Riziotis et al., 2008) and aircraft wings (Cesnik et al., 2014) are now well known. Although these effects can be modeled in some aeroelastic tools by using geometric nonlinear structural solvers (Larsen and Hansen, 2019; DNV, 2016; Wang et al., 2017; Bauchau, 2009) where the stiffness matrix terms are function of deflections or in other words nonlinear, linear modal based ROMs are still in use even for structures with large deflections such as wind turbine blades (Branlard, 2019; Jonkman and Buhl Jr, 2005; Branlard and Geisler, 2022) due to their speed. Therefore, it is very desirable to increase accuracy with negligible extra computational demand for such tools. This is fully aligned with the main focus of the present work.

The focus of this study is cantilever beam structures and their reduced order models (ROMs) based on modal approach used in coupled simulations such as aeroelasticity and load simulation of wind turbines and aircraft. A new correction method for moderately large bending deflection effects is proposed for modal based ROMs. The method has possible minimum computational cost during the coupled analysis since it includes only some correction terms which don't require any extra iteration during the response analysis.

There are many studies in the literature on geometrically nonlinear ROMs and most of them focus on clamped-clamped beams or simply supported panels. Table 1 shows some prominent works with cantilever structures from the literature together with the methods and examples used in them. The methods shown in Table 1 are either intrusive or non-intrusive. In the former, the nonlinear stiffness matrix terms in modal space are derived analytically. While the latter assumes a cubic relation between modal amplitudes and internal forces and the coefficients are determined with static analysis. As shown in the table, most of the work uses Von karman kinematics which are very useful for deriving the nonlinear stiffness terms as a function of displacements and it captures the moderately large deflections accurately when plate or shell elements are used.

Intrusive and non-intrusive methods require reduction bases where the displacements are nonlinear function of modal amplitudes. In the given studies a quadratic relation between displacements and modal amplitudes are used with modal derivatives or expansion modes which are called "dual modes" in some studies. All of these studies, except Gözcü and Dou (2020) are limited to beam models with forces applied in single direction or forces in two bending direction with bending deflections less than $2\,\%$ of beam span. Moreover, the methods used in existing studies require much more computational time than linear ROMs due to the iterative solutions required by nonlinear stiffness matrices. On the other hand, our proposed method uses linear reduction basis and linear stiffness matrix for computing deflections and corrects the linear deflections results with some quadratic vectors for capturing large bending deflection effects. It may be less accurate compared to the ROMs with nonlinear stiffness terms, however it has a very similar computational speed to the existing linear ROMs and easy to implement to existing aeroelastic tools compared to nonlinear models.

The focus of nonlinear ROMs in the literature is generally to use the same model for response and stress analysis. On the other hand, this study aims to come with a fast and accurate ROM correction method that is suitable only for response analysis and not for stress analysis. The main contributions of this paper are:

- Selection of the important physics for the given applications and thus justification of particular method choice (i.e. displacement only correction).

- Proof of method suitability using a high-fidelity model with prescribed external loads on both simple and complex geometries.

The paper is divided into three four sections. The kinematics of cantilever beam problem relevant to this study is explained in Section 2 and the proposed method is explained in Section 3. Example cases are introduced and their results are given together with discussion in Section 4 and the conclusion takes place in Section 5.

Table 1. Overview of the studies with cantilever structure models. The methods, reduction bases and example cantilever structures used in the reference studies are given together with applied forces and maximum deflections in terms of span length.

Reference	Method	Reduction basis	Example structure	Force direction	Max. deflection
Kim et al. (2009)	Displacement based Non-intrusive with von Karman kinematics	Bending modes + expansion modes	2D straight beam	1 bending direction	50% of span
Wang et al. (2013)	Displacement based Non-intrusive with von Karman kinematics	Bending modes + expansion modes	An unmanned aircraft wing	1 bending direction	25% of span
Jain et al. (2017)	Intrusive with von Karman kinematics	Quadratic basis & Modal derivatives	A wing model	1 bending direction	2% of span
Rutzmoser et al. (2017)	Intrusive with von Karman kinematics	Different quadratic bases	2D straight beam	1 bending direction	30% of span
Wu et al. (2018)	Intrusive with von Karman kinematics	Rubin basis + Modal derivatives	NREL 5MW blade	2 bending direction	1% of span
Gözcü and Dou (2020)	Force based Non-intrusive	Linear modes + Modal derivatives	3D straight beam NREL5MW blade	2 bending directions	10-20% of span
This study	Linear approach Correction terms	Linear modes	3D straight beam IEA15MW blade	2 bending directions	20% of span

2 Relevant Kinematics

This section explains the kinematics of cantilever beams and geometric nonlinear effects due to large bending deflections for symmetric beams and initially curved beams such as wind turbine blades.

Although there are many research studies about geometrically nonlinear ROMs, most of them focus on clamped-clamped beams or simply-supported plates. In clamped-clamped case, the nonlinearity arises due to the length change where a lateral deflection actually alters the length of the structure which causes an additional stiffness effect such as hardening or softening depending on the sign of length change. This effect is referred to as membrane effect or bending-extension coupling (Touzé et al., 2021). In the case of cantilever beams, a lateral deflection due to lateral forces doesn't result in length change (no axial strain), so there is no bending-extension coupling for cantilever beams. However, the free end of a cantilever beam displaces in the beam span direction to keep the length constant when it bends as shown in Figure 1. In other words, the cantilever beams with lateral loading go through large rotations which don't result in any strain.
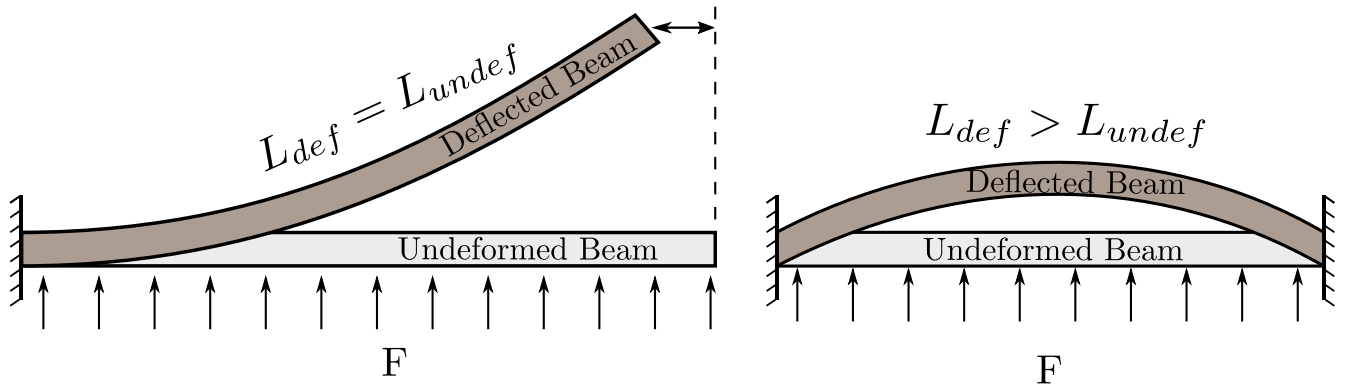
Figure 1. Displacements of a cantilever and a clamped-clamped beam under lateral distributed loads F. The deflected beam length (L_{def}) is equal to the undeflected length (L_{undef}) for the cantilever beam, resulting in zero axial strain. The clamped-clamped beam has axial strain due to elongation in beam length.

The cantilever beam in its deflected state can display a bending-torsion coupling behavior that is not seen in the undeflected state of the straight symmetric cantilever beam. Figure 2 depicts these kinematics using a straight cantilever beam. The lateral force (F_x) deflects the beam to *State-1*. Subsequently, the force perpendicular to F_x is applied on the beam which is now at *Final State*. It is observed that the beam deflects not only laterally and vertically but also in the torsion direction, even though there is no torsion load. Geometrically linear models (such as ROMs based on modal approach) can capture bending deflections but not the torsion deflection for this problem since their stiffness matrices are not updated by new states or deflections.
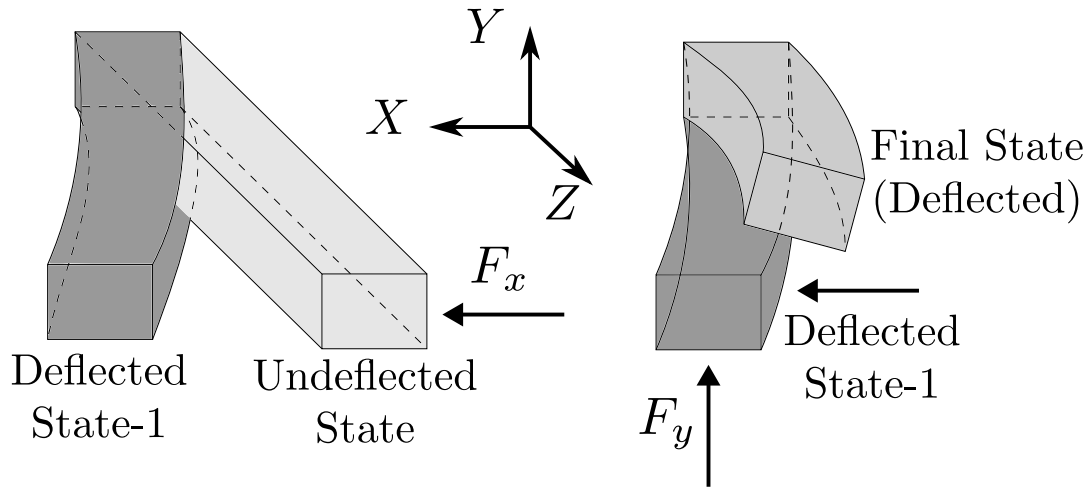
Figure 2. Illustration of beam deflections in lateral directions and the resulting torsion motion due to the bending/torsion coupling at the deflected state. The lateral ($x-$, $y-$) and axial ($z-$) directions are given in beam root coordinates.

These kinematics become even more prominent for applications such as wind turbine blades which are initially curved structures due to prebend. They have already bending/torsion couplings at their undeflected states but the lateral deflections change the magnitude as well as the direction of this coupling. Figure 3 shows the torsion deflection due to the combination of flapwise and edgewise deflections of a wind turbine blade with prebend at its undeflected position. The edgewise and torsion motions are already coupled for a blade with prebend as shown in the figure. However this coupling first reduces and then changes sign with flapwise bending deflections. As the blade goes through sinusoidal edgewise bending deflections due to gravity and rotation, the torsion induced by edgewise-torsion coupling also alters blade loads and aeroelastic stability (Kallesøe, 2011). These coupling effects become significant for very flexible wind turbine blades. In case geometrically linear models like classical ROMs based on modal reduction are used, the change of torsion-edgewise coupling cannot be captured correctly for large blade deflections.
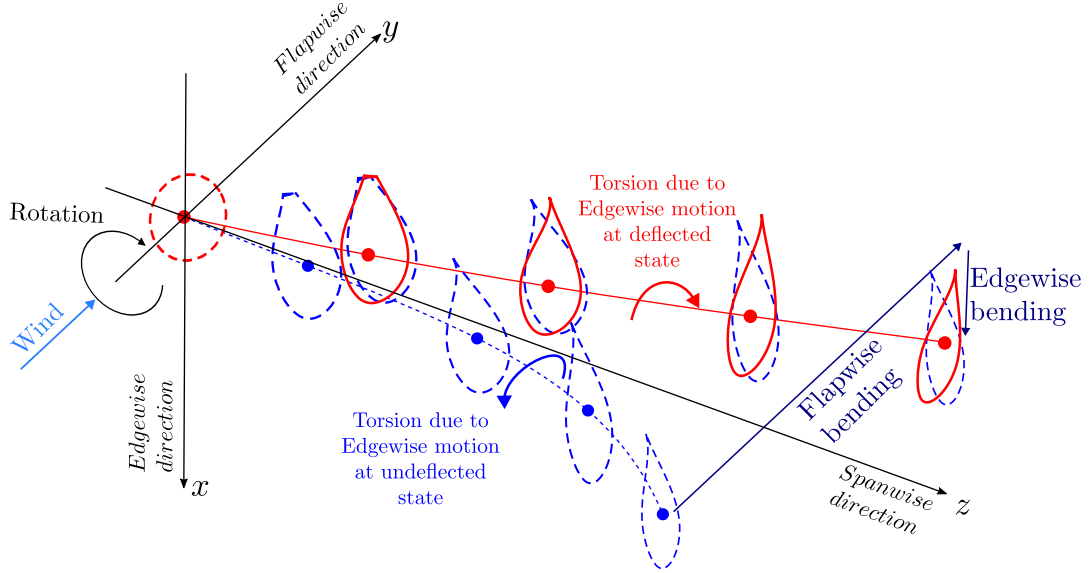
Figure 3. Illustration of a wind turbine deflections in flapwise ($y-$) and edgewise ($x-$) directions and the resulting torsion motion due to the bending/torsion coupling at the deflected state. The lateral ($x-$, $y-$) and axial ($z-$) directions are given in blade root coordinates. The effective blade length is the projected length onto the root coordinate system in the axial direction. The edgewise/torsion coupling at the initial blade position has an opposite direction in comparison to the edgewise/torsion coupling at the deflected blade position.

Here, the kinematics of a cantilever beam due to bending deflections are explained and kinematics due to axial-bending coupling is left without mentioning since the proposed method is developed only for secondary effects due to large bending deflections of cantilever beams. Hence, the method cannot capture stiffening effects with centrifugal force (Wallrapp and Schwertassek, 1991; Branlard and Geisler, 2022) which comes from bending-extension coupling. However, centrifugal stiffening is already corrected for linear models in existing tools such as FLEX (Branlard, 2019), FAST (Jonkman and Buhl Jr, 2005). In this study, mode shapes at undeformed state without centrifugal stiffening effects are used since the mentioned existing tools

compute blade mode shapes at undeflected states. However, the method is not limited with undeflected state modal analysis and it can also work with mode shapes computed at any deflected state.

3 Method

The nonlinear geometric effects of a cantilever beam can be captured by nonlinear ROMs using different methods (Intrusive or Non-intrusive see Table 1) and reduction basis where linear modes are used together with quadratic vectors such as `Expansion modes` (Hollkamp and Gordon, 2008) or `Modal derivatives` (Idelsohn and Cardona, 1985). It is observed that effects of nonlinear stiffness terms such as hardening/stiffening are not significant in bending directions for moderately large deflections of a cantilever beam. On the other hand, the geometric nonlinear effects explained in Section 2 are still apparent for cantilever beams.

These kinematics together with other nonlinear effects such as centrifugal stiffening are captured very accurately by geometrically nonlinear models which come with much higher computational cost compared to linear ROMs. Our method uses linear ROMs which use linear mode shapes, stiffness, mass and damping matrices for response calculation and quadratic vectors are added to the linear response results to capture large bending deflection effects. In the studies where intrusive methods are used, `Modal derivatives` are generally preferred as quadratic vectors for deriving nonlinear stiffness terms in modal space. For non-intrusive methods, the terms for cubic relation between modal amplitudes and reduced stiffness terms are obtained from some static solutions and the reduction basis includes generally `Expansion modes`. In this study, both `Modal derivatives` and `Expansion modes` are investigated as correction terms for large bending effects. The formulation and calculation process of these vectors are explained below.

3.1 Modal derivatives

The modal derivatives (MDs) are quadratic vectors which include secondary effects that occur due to large deflections (geometric nonlinearities) (Idelsohn and Cardona, 1985; Wu and Tiso, 2014). The quadratic relation needs to be written between physical displacements ($\boldsymbol{u}$) and modal amplitudes ($\boldsymbol{q}$) for defining modal derivatives. So, they can be thought of as second derivative of physical displacements ($\boldsymbol{u}$) with respect to modal amplitudes ($\boldsymbol{q}$) when the displacements are represented as a function of modal amplitudes. When Taylor series expansion of the displacements around an equilibrium state ($\boldsymbol{u}_0 = \boldsymbol{u}(\boldsymbol{q}_0)$) are written, the first term ($\boldsymbol{u}(\boldsymbol{q}_0)$) is the equilibrium state, the first derivative represents the linear mode shapes and the second derivative term includes the modal derivatives as shown in equation (1).

$$
\begin{aligned}
\boldsymbol{u}(\boldsymbol{q}) \approx & \boldsymbol{u}(\boldsymbol{q}_0) + \left.\frac{\partial \boldsymbol{u}}{\partial \boldsymbol{q}}\right|_{\boldsymbol{q}_0} \cdot (\boldsymbol{q} - \boldsymbol{q}_0) + \frac{1}{2}\left(\left.\frac{\partial^2 \boldsymbol{u}}{\partial \boldsymbol{q} \partial \boldsymbol{q}}\right|_{\boldsymbol{q}_0} \cdot (\boldsymbol{q} - \boldsymbol{q}_0)\right) \cdot (\boldsymbol{q} - \boldsymbol{q}_0) + \mathcal{O}(\|\boldsymbol{q}\|^3) \\
= & \boldsymbol{u}(\boldsymbol{q}_0) + \boldsymbol{\Phi} \cdot \boldsymbol{q} + \frac{1}{2}\left(\frac{\partial \boldsymbol{\Phi}}{\partial \boldsymbol{q}} \cdot \boldsymbol{q}\right) \cdot \boldsymbol{q} + \mathcal{O}(\|\boldsymbol{q}\|^3)
\end{aligned}
\tag{1}
$$

In this study, the equilibrium state is taken as the initial state where $\boldsymbol{u}_0 = 0$ (undeflected state) and equation (1) can be written in terms of mode shapes and their derivatives at the initial state as

$$\boldsymbol{u}(\boldsymbol{q}) \approx \boldsymbol{\Phi} \cdot \boldsymbol{q} + \frac{1}{2}\left(\frac{\partial \boldsymbol{\Phi}}{\partial \boldsymbol{q}} \cdot \boldsymbol{q}\right) \cdot \boldsymbol{q} + \mathcal{O}(\|\boldsymbol{q}\|^3) \tag{2}$$

where $\boldsymbol{\Phi}$ is linear mode shapes , $\boldsymbol{u}$ is displacement vector and $\boldsymbol{q}$ is modal amplitude vector. The displacement vector is function of time (t) and position (x), whereas mode shapes are only function of position (x) and modal amplitudes are only function of time (t). So, they can be written as $\boldsymbol{u}(t,x)$, $\boldsymbol{q}(t)$, $\boldsymbol{\Phi}(x)$, however their time and position relations are not included in the equations for simplicity. The linear mode-shapes ($\boldsymbol{\Phi}$) and corresponding natural frequencies (ω) can be found by the generalized eigenvalue solution,

$$(\boldsymbol{K} - \omega_i^2 \boldsymbol{M})\boldsymbol{\phi}_i = \boldsymbol{0} \tag{3}$$

where $\boldsymbol{K}$, $\boldsymbol{M}$ are the tangent stiffness and mass matrices and ω_i, $\boldsymbol{\phi}_i$ are the ith eigenvalue and corresponding eigenvector (mode-shape vector). The tangent stiffness is the Jacobian of the internal force with respect to the displacement. It is a generalization of the linear stiffness matrix in the nonlinear case. Here the tangent stiffness and mass matrices are computed at the initial state ($\boldsymbol{u}_0 = 0$) for the purpose of solving eigenvalue problems. As seen in the later derivation in this section, the tangent stiffness at the deflected state is also required to compute the modal derivatives. The modal derivatives are calculated by taking the derivative of eigenvalue problem shown in equation (3) with respect to modal amplitude q_j.

$$\frac{\partial}{\partial q_j}\left((\boldsymbol{K} - \omega_i^2 \boldsymbol{M})\boldsymbol{\phi}_i\right) = \left(\frac{\partial \boldsymbol{K}}{\partial q_j} - \frac{\partial \omega_i^2}{\partial q_j}\boldsymbol{M} - \omega_i^2\frac{\partial \boldsymbol{M}}{\partial q_j}\right)\boldsymbol{\phi}_i + (\boldsymbol{K} - \omega_i^2 \boldsymbol{M})\frac{\partial \boldsymbol{\phi}_i}{\partial q_j} = 0 \tag{4}$$

To determine the derivative of $\boldsymbol{\phi}_i$ and ω_i with respect to the jth modal amplitude q_j, another equation is needed. This equation can be chosen as equation (5) where $\boldsymbol{\phi}_i$ is the mass normalized mode shape vector.

$$\frac{\partial}{\partial q_j}(\boldsymbol{\phi}_i^T \boldsymbol{M} \boldsymbol{\phi}_i) = 2\boldsymbol{\phi}_i^T \boldsymbol{M}^T \frac{\partial \boldsymbol{\phi}_i}{\partial q_j} + \boldsymbol{\phi}_i^T \frac{\partial \boldsymbol{M}}{\partial q_j}\boldsymbol{\phi}_i = 0, \text{ where } \boldsymbol{\phi}_i^T \boldsymbol{M} \boldsymbol{\phi}_i = 1 \tag{5}$$

When the equation (4) and (5) are combined, the modal derivative of ith mode shape vector $\boldsymbol{\phi}_i$ and natural frequency ω_i with respect to the jth modal amplitude can be determined by

$$\begin{bmatrix} (\boldsymbol{K} - \omega_i^2 \boldsymbol{M}) & -\boldsymbol{M}\boldsymbol{\phi}_i \\ -(\boldsymbol{M}\boldsymbol{\phi}_i)^T & 0 \end{bmatrix}\begin{bmatrix} \dfrac{\partial \boldsymbol{\phi}_i}{\partial q_j} \\ \dfrac{\partial \omega_i^2}{\partial q_j} \end{bmatrix} = \begin{bmatrix} -\dfrac{\partial \boldsymbol{K}}{\partial q_j}\boldsymbol{\phi}_i + \omega_i^2\dfrac{\partial \boldsymbol{M}}{\partial q_j}\boldsymbol{\phi}_i \\ \frac{1}{2}\boldsymbol{\phi}_i^T \dfrac{\partial \boldsymbol{M}}{\partial q_j}\boldsymbol{\phi}_i \end{bmatrix} \tag{6}$$

Equation (6) contains all the terms that are required to compute the modal derivatives. The derivation of modal derivatives is similar to the derivation of the sensitivity of eigenmodes and eigenfrequencies with respect to a design variable in structural optimization.

For computation of modal derivatives, the terms related to inertia effects (i.e. mass matrix and its derivatives) are generally ignored, since their contribution to the modal derivatives is very limited (Rutzmoser et al., 2017). The derivative of the eigenvalue can also be assumed to be zero due to the fact the eigenfrequencies of the slender cantilever beams are not sensitive to

the vibration amplitude. These assumptions lead to static modal derivatives which are symmetric whereas modal derivatives computed from equation (6) are not necessarily symmetric.

$$\frac{\partial \phi_i}{\partial q_j} = -\boldsymbol{K}^{-1}\frac{\partial \boldsymbol{K}}{\partial q_j}\phi_i \tag{7}$$

For conciseness, the static modal derivatives are simply called 'Modal Derivatives (MDs)' hereafter. In equation (7), the derivative of the stiffness matrix with respect to the jth modal amplitudes, i.e. $\frac{\partial \boldsymbol{K}}{\partial q_j}$, is needed to compute the modal derivatives. In this study, the derivative of stiffness matrix ($\boldsymbol{K}$) with respect to the jth modal amplitudes (q_j) is computed by central finite differences as

$$\frac{\partial \boldsymbol{K}}{\partial q_j} = \frac{\boldsymbol{K}(\phi_j\delta_j) - \boldsymbol{K}(-\phi_j\delta_j)}{2\delta_j} \tag{8}$$

where $\boldsymbol{K}(\phi_j\delta_j)$ is the tangent stiffness matrix when the system displacements equals to $\phi_j\delta_j$. The tangent stiffness matrix at the deflected state of the structure by a given amplitudes of δ_j is computed with a geometrically non-linear beam solver based on co-rotational formulation in (Krenk, 2005). The calculation of $\frac{\partial \boldsymbol{K}}{\partial q_j}$ from equation (8) is the only step where a geometrically nonlinear solver is required. When the stiffness matrix derivatives are ready, the computation of equation (7) is straightforward since the rest of the equation consists of stiffness matrix and linear eigenvectors at the undeflected state. The tangent stiffness matrix at undeflected state is actually the linear stiffness matrix which is used in existing modal approaches. There are (M_{MD}) number of modal derivatives which are computed for M number of linear mode-shapes. The relation between M and M_{MD} can be written as,

$$M_{MD} = \frac{M \times (M+1)}{2} \tag{9}$$

Figure 4 and 5 are used to give visual understanding of the modal derivatives. Figure 4 shows bending of a straight beam with airfoil cross-section in one direction and its representation by a linear bending mode and its modal derivative by itself. The linear bending mode shape doesn't have any displacement in axial (span-wise) direction, so the total (curved) length of the beam increases. The modal derivative vector of the bending mode-shape with respect to its modal amplitude includes axial displacement effect. When the linear bending mode and its modal derivative is summed, the axial displacement and bending effects are captured together.
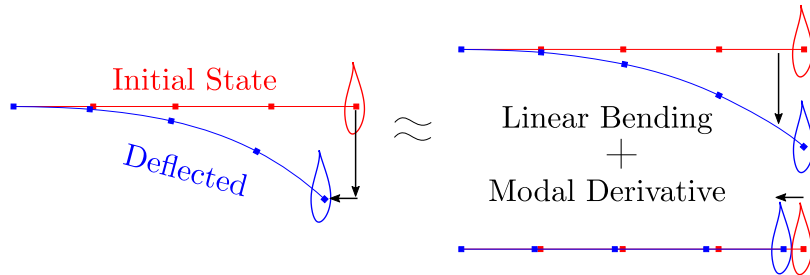
Figure 4. Bending deflection of a straight beam in the first mode shape and its representation by linear mode shape and its modal derivatives.

Figure 5 shows the modal derivatives that are similar to that in Figure 4 except that the deflections occur in two bending directions at the same time. Hence, together with the axial displacements, there is also a torsion effect due to the couplings at the deflected state. The linear modal approach is only capable of capturing the bending deflections in two lateral ($x-$ and $y-$) directions. The axial displacements are captured by the modal derivatives of each bending mode shape with respect to its own modal amplitudes in Figure 5, whereas the torsion effects are included in the cross modal derivative vectors which are the derivatives of one bending mode-shape with respect to the modal amplitudes of another bending mode in the other direction.
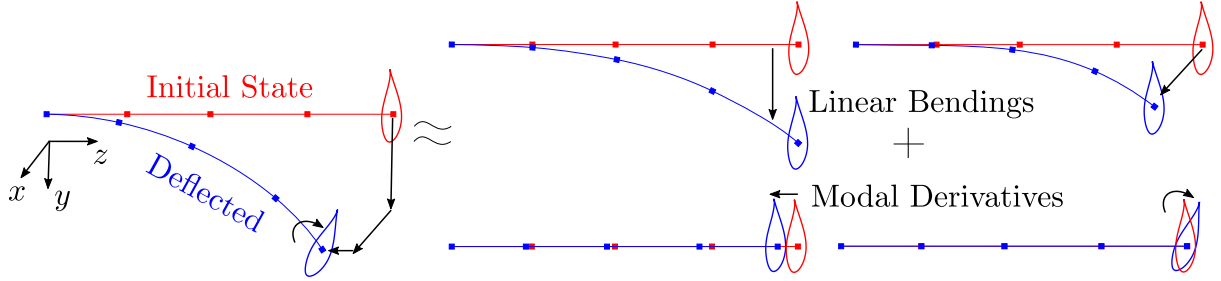
Figure 5. Bending deflections of a straight beam in lateral ($x-$ and $y-$) directions and the representation of the deflections by linear mode shapes and their modal derivatives.

3.2 Expansion modes

Expansion modes are similar to modal derivatives, but they are computed by a non-intrusive approach (Hollkamp and Gordon, 2008). The expansion modes also contain the secondary effects such as the axial and torsion motions caused by the bending motions. These vectors are computed from the difference between the deflections computed by linear ROMs and the nonlinear deflections. The difference is written as a function of selected order of modal amplitudes and a quadratic (2nd order) relation is used in this study. Nonlinear deflections for static cases are computed in a geometrically non-linear solver. In the expansion mode approach, the physical displacements are represented as

$$\boldsymbol{u}(t,x) \approx \boldsymbol{\Phi}(x)\boldsymbol{q}(t) + \boldsymbol{\Phi}_{EM}(x)\,\boldsymbol{q}_{EM}(t) \tag{10}$$

where $\boldsymbol{\Phi}$ and $\boldsymbol{\Phi}_{EM}$ are the matrices whose columns are the linear modes and the expansion modes, x is position and t is time. The expansion mode amplitudes $\boldsymbol{q}_{EM}$ are quadratic functions of the bending modes, and can be written in terms of the M linear mode amplitudes as

$$\boldsymbol{q}_{EM} = \begin{bmatrix} q_1^2 & q_1 q_2 & \dots & q_1 q_M & q_2^2 & q_2 q_3 & \dots & q_{(M-1)} q_M & q_M^2 \end{bmatrix}^T \tag{11}$$

where the q_i is the ith linear mode amplitudes. The relation between the number of linear modes (M) and the number of corresponding expansion modes (M_{EM}) is

$$M_{EM} = \frac{M \times (M+1)}{2} \tag{12}$$

So, there are the same number of modal derivatives and expansion modes for the same number of linear modes, since both of these vectors represents the quadratic relation between deflections and modal amplitudes.

While the above Equation 10 defines the expansion modes, the procedure to compute the expansion modes are given below.

First, a set of static analyses are performed with a geometrically nonlinear solver. The applied forces are chosen as a combination of two linear modal shapes ($\mathbf{\Phi}$), which can be written as

$$\boldsymbol{f} = \boldsymbol{K}(\lambda_i \mathbf{\Phi}_i + \lambda_j \mathbf{\Phi}_j) \tag{13}$$

where λ_i and λ_j are force amplifiers for i^{th} and j^{th} linear mode-shape. The non-linear displacements ($\boldsymbol{u}$) are computed by a co-rotational beam solver for a set of static loads $\boldsymbol{f}$.

Second, the amplitudes of the linear modes, i.e. $\boldsymbol{q}$, are computed from the applied loads as

$$\begin{aligned}\mathbf{\Phi}^T \boldsymbol{K} \mathbf{\Phi} \boldsymbol{q} = \mathbf{\Phi}^T \boldsymbol{f} = \boldsymbol{K_r} \boldsymbol{q} = \boldsymbol{f_r} \\ \boldsymbol{q} = \boldsymbol{K_r}^{-1} \boldsymbol{f_r}\end{aligned} \tag{14}$$

where $\boldsymbol{K}$ and $\boldsymbol{K_r}$ are the full and reduced stiffness matrices, and $\boldsymbol{f}$ and $\boldsymbol{f_r}$ are the full and reduced force vectors. When the applied forces ($\boldsymbol{f}$) are known, $\boldsymbol{q}$ can be computed.

Once we have the linear modal amplitudes ($\boldsymbol{q}$), the corresponding expansion modal amplitudes ($\boldsymbol{q}_{EM}$) can be computed by using equation (11).

Then, the nonlinear displacements, the amplitudes of the linear modes, and the amplitudes of the expansion modes can be collected into three matrices: $\boldsymbol{U} \in \mathbb{R}^{N \times N_k}$, $\boldsymbol{Q} \in \mathbb{R}^{M \times N_k}$ and $\boldsymbol{Q}_{EM} \in \mathbb{R}^{M_{EM} \times N_k}$. Here each column of the matrices corresponds to a static load case. All load case results can be written in matrix form as

$$\boldsymbol{U} \approx \mathbf{\Phi}\boldsymbol{Q} + \mathbf{\Phi}_{EM}\boldsymbol{Q}_{EM} \tag{15}$$

Equation (15) is similar to Equation (10) except that Equation (15) is in matrix form where the nonlinear displacements $\boldsymbol{U}$, the linear modes $\mathbf{\Phi}$, the amplitudes of the linear modes $\boldsymbol{Q}$, and the amplitudes of the expansion modes $\boldsymbol{Q}_{EM}$ are known from the above steps. The only unknown in Equation (15) is the expansion modes $\mathbf{\Phi}_{EM}$.

Finally, the expansion modes can be determined by using the least square method

$$\mathbf{\Phi}_{EM}\boldsymbol{Q}_{EM} = \boldsymbol{U} - \mathbf{\Phi}\boldsymbol{Q} \longrightarrow \underset{\mathbf{\Phi}_{EM} \in \mathbb{R}^{N \times M_{EM}}}{\text{minimize}} \|\boldsymbol{U} - \mathbf{\Phi}\boldsymbol{Q} - \mathbf{\Phi}_{EM}\boldsymbol{Q}_{EM}\| \tag{16}$$

where $\| \ \|$ denotes the 2-norm of the vector and it is solved for Modal expansion matrix $\mathbf{\Phi}_{EM}$.

It is noted that the expansion modes are very similar to the modal derivatives. They are identical except the numeric differences if the set of ith and j^{th} are symmetric and the force amplitudes λ_i and λ_j are small enough. The computational cost of the expansion modes is more expensive than the modal derivatives since their calculation requires more static solutions than the calculation of the modal derivatives. The difference in the computational cost is small when the number of linear modes (M) is small. However, the computational cost difference becomes significant when the number of the linear modes is large.

Further, it is noted that one can extend Equation (11) to include higher-order expansion modes corresponding to higher-order polynomial terms of the amplitudes of the linear modes, for example, the expansion modes for the cubic and quartic terms.

3.3 Numerical implementation

As mentioned before, modal derivatives or expansion mode-shapes are not included into the reduction space and linear mass, stiffness and damping matrices are used for the response analysis. This isn't the case for other studies in the literature (see Table 1) which use nonlinear stiffness terms in modal space. Algorithm 1 shows the procedure to obtain structural response with quadratic correction vectors for pure structural response analysis where the forces function of only time and for coupled response analysis where the forces are function of both time and displacements. In this study, modal derivative and expansion mode vectors are used as quadratic correction vectors.

Algorithm 1 Response calculation with quadratic correction vectors

---

- Model generation step (time independent and done once)

    1. Generate linear ROM from finite element model:

        (a) Compute mode-shape vectors ($\boldsymbol{\phi}_i$) from $\boldsymbol{K} - \omega_i^2 \boldsymbol{M})\boldsymbol{\phi}_i = \boldsymbol{0}$

        (b) Compute reduced order stiffness $\boldsymbol{K_r}$, mass $\boldsymbol{M_r}$ and damping $\boldsymbol{C_r}$ matrices by Galerkin projection :
        $\boldsymbol{K_r} = \boldsymbol{\Phi}^T \boldsymbol{K} \boldsymbol{\Phi}, \boldsymbol{M_r} = \boldsymbol{\Phi}^T \boldsymbol{M} \boldsymbol{\Phi}, \boldsymbol{C_r} = \boldsymbol{\Phi}^T \boldsymbol{C} \boldsymbol{\Phi}$

    2. Compute quadratic vectors:
        For modal derivatives see section 3.1
        For expansion modes see section 3.2

- Pure structural response analysis (force is function of only time)

    1. Compute modal amplitudes for linear ROM by solving equation of motion:
        $\boldsymbol{M_r} \ddot{\boldsymbol{q}}(t) + \boldsymbol{C_r} \dot{\boldsymbol{q}}(t) + \boldsymbol{K_r} \boldsymbol{q}(t) = \boldsymbol{\Phi}^T \boldsymbol{f}(t) = \boldsymbol{f_r}(t)$

    2. Compute displacements by using linear mode-shapes, quadratic vectors and modal amplitudes :
        With MDs : $\boldsymbol{u}(x,t) = \boldsymbol{\Phi}(x) \cdot \boldsymbol{q}(t) + \frac{1}{2} \left(\frac{\partial \boldsymbol{\Phi}}{\partial \boldsymbol{q}} \cdot \boldsymbol{q}(t) \right) \cdot \boldsymbol{q}(t)$
        with EMs : $\boldsymbol{u}(x,t) = \boldsymbol{\Phi}(x) \boldsymbol{q}(t) + \boldsymbol{\Phi}_E(x) \, \boldsymbol{q}_E(q)$
        The calculation of displacements ($\boldsymbol{u}(x,t)$) doesn't have to be done at each time step and can be performed as a post process after the time simulations.

- Coupled response analysis (force is function of time and displacement)

    1. Compute modal amplitudes for linear ROM by solving equation of motion:
        $\boldsymbol{M_r} \ddot{\boldsymbol{q}}(t) + \boldsymbol{C_r} \dot{\boldsymbol{q}}(t) + \boldsymbol{K_r} \boldsymbol{q}(t) = \boldsymbol{\Phi}^T \boldsymbol{f}(t, \boldsymbol{u}) = \boldsymbol{f_r}(t, \boldsymbol{u})$

    2. Compute displacements by using linear mode-shapes, quadratic vectors and modal amplitudes :
        With MDs : $\boldsymbol{u}(x,t) = \boldsymbol{\Phi}(x) \cdot \boldsymbol{q}(t) + \frac{1}{2} \left(\frac{\partial \boldsymbol{\Phi}}{\partial \boldsymbol{q}} \cdot \boldsymbol{q}(t) \right) \cdot \boldsymbol{q}(t)$
        with EMs : $\boldsymbol{u}(x,t) = \boldsymbol{\Phi}(x) \boldsymbol{q}(t) + \boldsymbol{\Phi}_E(x) \, \boldsymbol{q}_E(q)$

    3. Update loads ($\boldsymbol{f}(t, \boldsymbol{u})$) and apply them

---

4 Results and Discussion

The proposed method is demonstrated in the case studies of a straight cantilever beam and the blade of the IEA 15MW reference wind turbine under static and dynamic loads. The displacement results are given to evaluate the effectiveness of the correction methods based on the modal derivatives and expansion modes to capture the large bending deflection effects. The reduced
5 order model results are compared with HAWC2 results for both static and dynamic cases. HAWC2 (Larsen and Hansen, 2019) is a aero-servo-hydro-elastic load analysis tool for wind turbines and developed by DTU Wind and Energy Systems. It uses multibody formulation with Timoshenko beam and can capture geometric non-linearities (Pavese et al., 2016). In HAWC2, $z-$ axis is along the axial direction whereas $x-$ and $y-$ directions are lateral directions (see Figure 3 for HAWC2 coordinate system).

10 ### 4.1 Straight beam

A cantilever straight beam model is used for static and dynamic load cases. Table 2 shows the general properties of the beam whose cross-section properties are constant along the beam length and shear coefficients are very high compared to the bending stiffness values, so it behaves like an Euler-Bernoulli beam.

Table 2. Straight beam geometry and cross-section stiffness properties. Beam is clamped from its root.

Length	Unit mass	EI_{xx}	EI_{yy}	GJ
$[m]$	$[kg/m]$	$[Nm^2]$	$[Nm^2]$	$[Nm^2]$
10.0	172.4	$215{\times}10^4$	$869{\times}10^3$	$416{\times}10^4$

Figure 6 shows $x-$, $y-$, $z-$ displacement and torsion motion components of the first two mode-shape vectors of the beam.
15 Since the beam is straight and has no material coupling, both bending mode-shapes have only one lateral direction displacement without any axial or torsion component. First mode-shape is in $x-$ direction and second one is in $y-$ direction.

Figure 7 shows modal derivative (MD) and expansion mode (EM) vectors for first two mode-shapes. The results are very similar for MD and EM vectors. These vectors show the sensitivity of a mode-shape with respect to a modal amplitude. The vector names are given so that the first number represents the mode number for linear mode-shape vector whose sensitivity is
20 computed with respect to the modal amplitude of the mode number which is given as the second number in the vector names. Hence, MD-1-1, MD-2-2, EM-1-1, EM-2-2 shows the sensitivity of a mode-shape with respect to its own modal amplitude whereas the MD-1-2 and EM-1-2 illustrate the sensitivity of a mode-shape with respect to another mode's modal amplitude. Since, MD-2-1 and MD-1-2 are same for static modal derivatives only MD-1-2 results are shown here. This symmetry case is also valid for expansion modes (EMs), since they are also computed for static cases. MD-i-i and EM-i-i vectors have only
25 axial displacements since their mode-shapes are only in one lateral direction. On the other hand, MD-i-j and EM-i-j have only torsion motions which represents the coupling between two lateral directions.
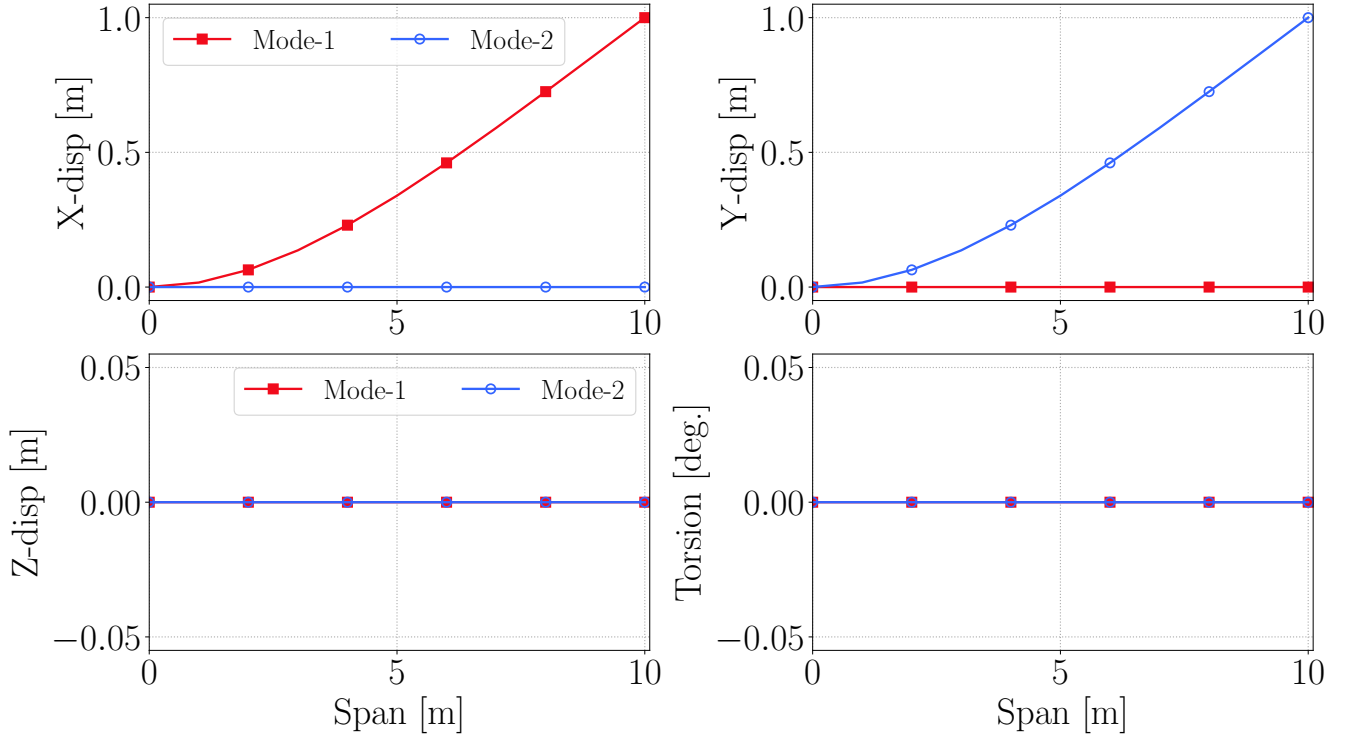
Figure 6. $x-$, $y-$, $z-$ and torsion components of first two mode shapes of straight beam. Beam span is along the $z-$ axis.

The first test was carried with static loads in $x-$ direction. The applied force vectors are determined from stiffness matrix ($\boldsymbol{K}$), first mode shape $\boldsymbol{\Phi}_1$ and amplification factor (λ) as,

$$\boldsymbol{F}_x = \lambda \boldsymbol{K} \boldsymbol{\Phi}_1 \tag{17}$$

where mode-shape $\boldsymbol{\Phi}_1$ is normalized according to its maximum value.

5   Expansion mode-shape and modal derivative results are same for this test case, therefore they are given together in Table 3 which shows the tip displacements for linear ROM without corrections (*Lin.*) and with modal derivative (*MD*) and expansion mode (*EM*) corrections and HAWC2 results. Modal derivative, expansion mode and linear ROM results are same for lateral ($x-$) deflections since uncoupled mode-shape result in zero values in lateral direction components (see Figure 7) of modal derivative and expansion mode vectors. Linear ROM error in $x-$ direction increases as the deflections increases and the error

10   is less than 5% for deflections of 20% beam length. Moreover linear model cannot capture any axial ($z-$) displacement whereas correction factors work quite well. The axial ($z-$) deflection is a secondary effect and captured by corrections coming from modal derivatives and expansion modes whereas linear model estimates zero displacement in $z-$ direction and 100% error for all solutions. Modal derivative and expansion mode errors are increasing by deflections and are much larger than bending ($x-$)
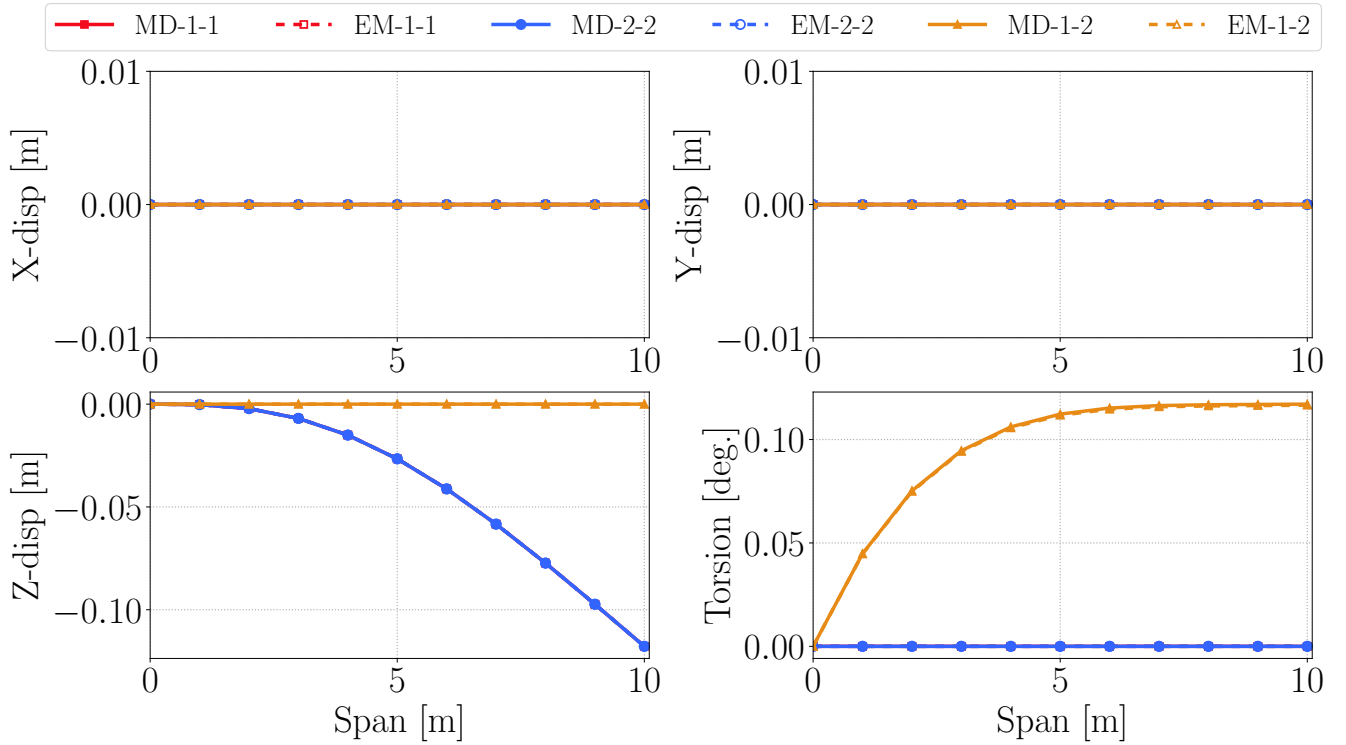
Figure 7. $x-$, $y-$, $z-$ and torsion components of modal derivative and expansion mode vectors. Beam span is along the $z-$ axis.

direction errors. The two main source of errors in secondary ($z-$) direction are truncation errors coming from eq. 2 and the error in bending ($x-$) direction which is even amplified for secondary effects due to the formulation.

Table 3. Straight beam lateral ($x-$) and axial ($z-$) tip deflection results for HAWC2, linear model, MD and EM corrections together with the errors of the models compared to HAWC2.

λ	x-HAWC2	x-Lin./MD/EM	x-error	z-HAWC2	z-MD/EM	z-MD/EM-err.	z-Lin.	z-Lin.-err.
1	0.991	1.000	0.9%	-0.057	-0.059	3.51%	0.0	100%
2	1.933	2.000	3.35%	-0.218	-0.236	8.26%	0.0	100%
3	2.790	3.000	7.0%	-0.459	-0.530	15.47%	0.0	100%

Figure 8 shows $x-$ and $z-$ (axial) positions of the structural nodes computed from HAWC2, linear ROM, MD and EM models for $\lambda = 2$ and $\lambda = 3$ load cases. The quadratic corrections capture the secondary effects all along the beam length.

5   The second test case include static loads in $x-$ and $y-$ directions. The load components are determined by similar formulation given in equation (17). The $x-$ force components are amplified by $\lambda = 2.5$ and the $y-$ force components are amplified by $\lambda = 1.0$. Figure 9 shows $x-$, $y-$, $z-$ displacements and torsion deflections along the beam length. Linear model estimates
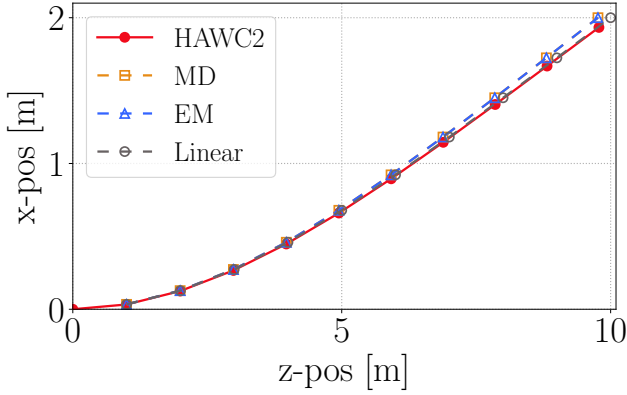
(a) Lateral and axial positions for $\lambda = 2$ deflections   (b) Lateral and axial positions for $\lambda = 3$ deflections
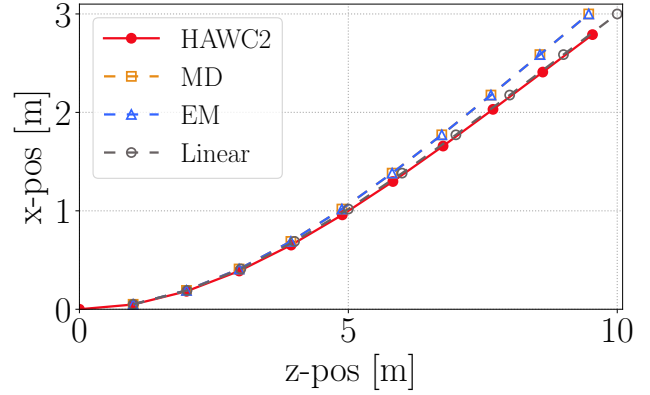
Figure 8. Straight beam $x-$ and $z-$ (axial) positions for $\lambda = 2$ and $\lambda = 3$ load cases. The positions are shown for HAWC2, linear ROM, MD and EM corrections.

$x-$ and $y-$ displacements quite accurately and quadratic vectors don't alter results in these directions since they don't have components in these directions (see Figure 7). On the other hand they capture the secondary effects in $z-$ and torsion directions due to geometric nonlinearities. Linear ROM cannot capture any axial ($z-$) displacements and torsion deflections. On the other hand, MD and EM corrections result in accurate estimation of secondary effect even though the loads are applied in two

5   directions. Hence, they can also capture the couplings between different directions.

The last load case with straight beam model includes dynamic loads in two lateral directions. The $x-$ direction load is constant with $\lambda = 2$ whereas the $y-$ direction load is computed as,

$$\boldsymbol{F}_y(t) = \boldsymbol{M}\boldsymbol{g}\sin(\omega t) \tag{18}$$

where $\boldsymbol{M}$ is mass matrix, $\boldsymbol{g}$ is acceleration vector, ω is a given rotation frequency of the rotor. Note that the beam does not

10   rotate, only the load varies with the given frequency. So, there is no axial ($z-$) force due to centrifugal effects. For this example the gravity vector has only $y-$ acceleration with value of $9.81 \; m/s^2$, and ω is taken as $1 \; rad/s$. The simulation time step is 0.01 seconds.

Figure 10 shows tip $x-$, $y-$, $z-$ displacements and torsion deflections for 100 seconds. Linear model can capture dynamics in $y-$ direction very accurately, and its $x-$ direction results are very close to HAWC2 results without any fluctuations after

15   60 seconds which cannot be captured without nonlinear stiffness terms Gözcü and Dou (2020). However these fluctuations are very small compared to the overall displacements in $x-$ direction. On the other hand, linear ROM results are again zero in axial and torsion directions whereas MD and EM corrections work very well even for initial transition period. Moreover, there is no phase difference between HAWC2 and MD/EM results which support that the nonlinear stiffness effects are very small for cantilever beams with moderate deflections. The fluctuations in $x-$ direction due to nonlinear stiffness term effects shows

20   the limitation of this method even though the fluctuations are very small.
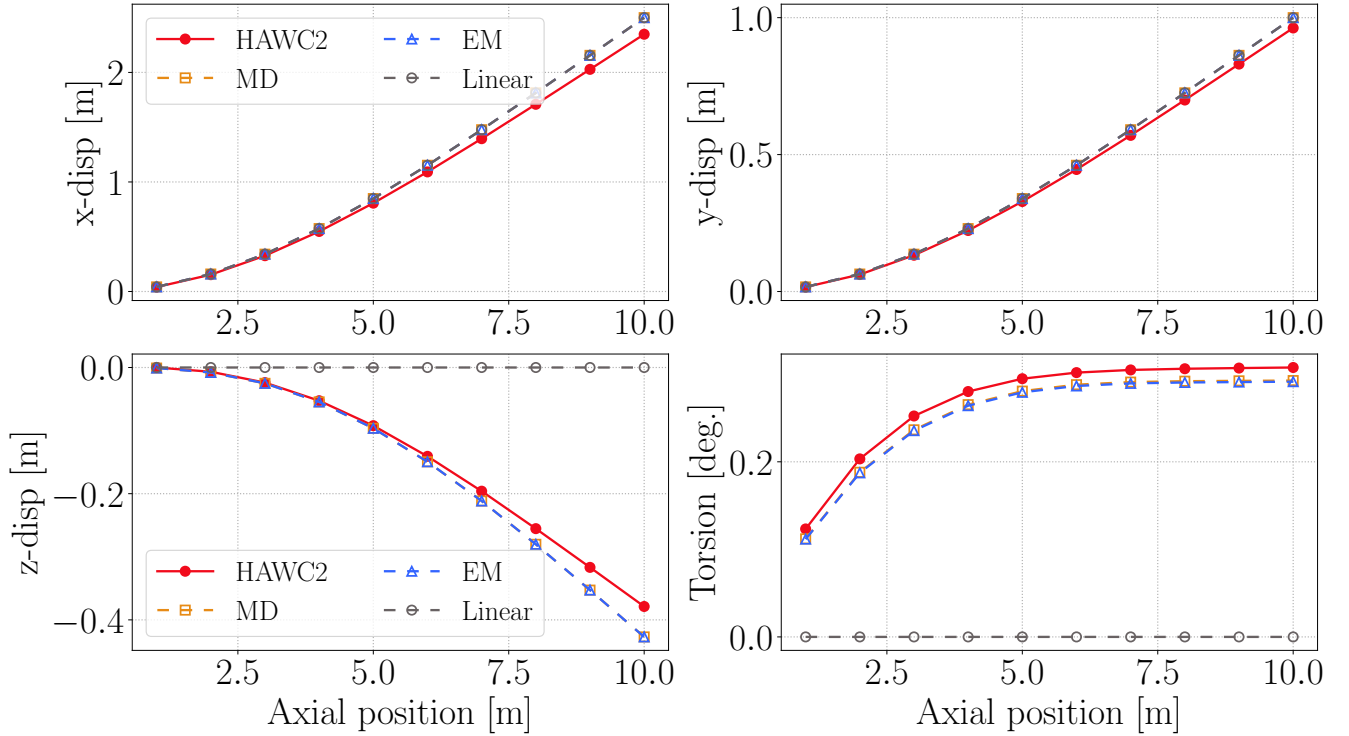
Figure 9. Straight beam $x-$, $y-$, $z-$ displacements and torsion motion results along the beam span. The static load has $x-$ and $y-$ components.

4.2 IEA 15MW turbine blade

The blade of the IEA 15MW wind turbine is modeled as beams in HAWC2 and FAST for load analysis Gaertner et al. (2020). It is a more complex structure in comparison to the beam studied in the previous section. The blade has material coupling terms and initially curved shape due to prebend (mostly in $y-$ direction), aerodynamic twist and backswept (mostly in $x-$ direction). Hence, the blade mode-shapes are coupled in $x-$, $y-$, $z-$ and torsion direction unlike the straight beam example. Besides, its cross-section stiffness properties change over the span and material couplings between lateral bending directions and torsion brings additional couplings in mode-shapes. Table 4 shows the relevant blade properties.

Table 4. IEA 15MW reference wind turbine blade: geometric dimensions, mass, and initial curvature limits in the prebend $(y-)$ and twist directions.

Length	Mass	Tip prebend	Max chord	Twist range
$[m]$	$[ton]$	$[m]$	$[m]$	$[deg]$
117	44.7	4.00	5.77	-15 to 2
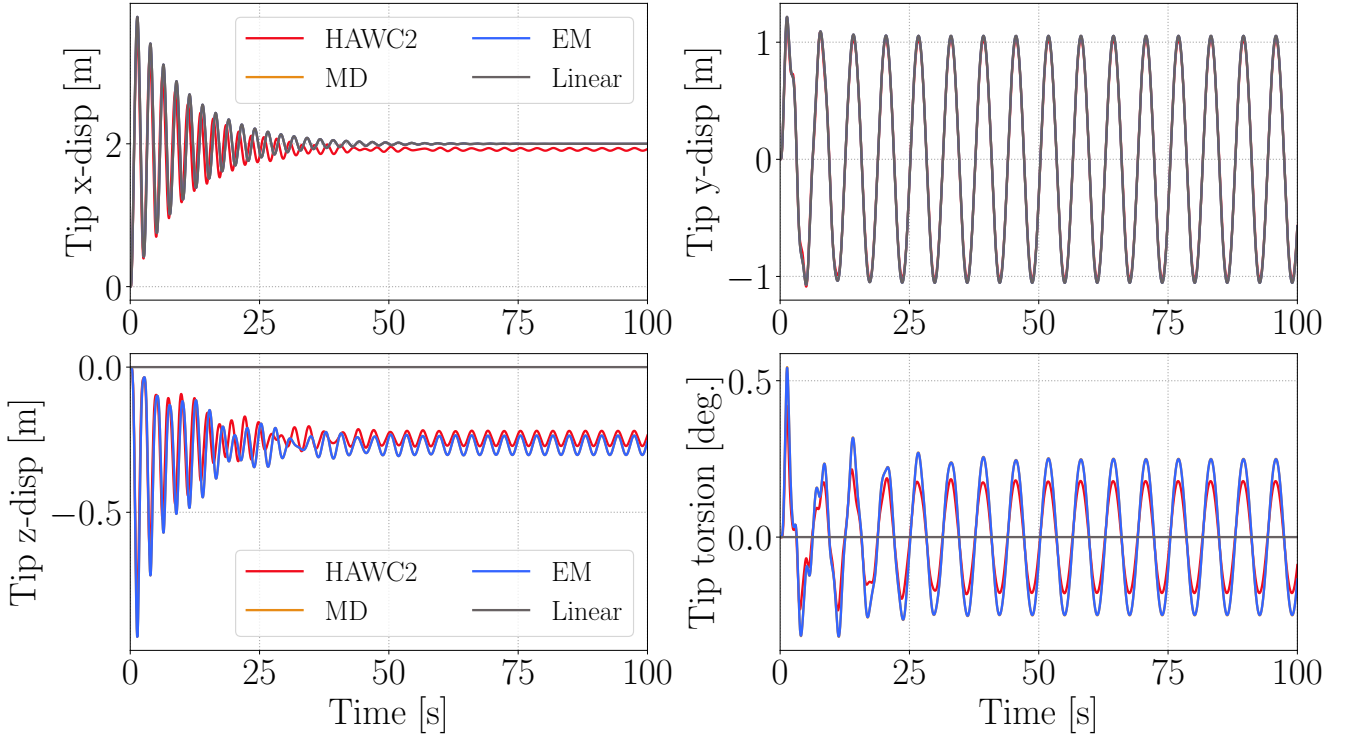
Figure 10. Straight beam dynamic analysis tip $x-$, $y-$, $z-$ displacements and torsion deflections for HAWC2, linear ROM, MD and EM corrections.

The straight beam example mode-shapes are uncoupled so that mode-shape vectors include non-zero values only in one lateral bending direction. However, the mode shapes of the turbine blade are coupled due to its geometry and cross-section material couplings. Figure 11 shows first two mode-shapes of the blade. The first mode-shape of the blade is mainly in $y-$ (flapwise) direction with $0.5\,\text{Hz}$ whereas the second mode-shape is mainly in $x-$ (edgewise) direction with around $0.7\,\text{Hz}$. Moreover, both mode-shapes have components in all directions including $z-$ (axial) and torsion directions. Second mode-shape torsion coupling is much stronger than the first mode-shape's coupling whereas it has weaker coupling in axial direction than the first mode-shape.

Figure 12 shows $x-$, $y-$, $z-$ and torsion components of modal derivative and expansion mode vectors for first two mode-shapes. MD and EM vectors are very similar and they include components in all directions due to the couplings. The difference between MD and EM vectors comes from numerical computation process. As seen in section 3.2, expansion modes (EM) are computed via least square method which uses all displacement and modal amplitude results gathered in matrices whereas each modal derivative (MD) is computed independently. Since the IEA 15MW reference wind turbine blade mode shapes are coupled, there are non-zero values at off-diagonal terms in the displacement matrices used during the computation of EMs. This leads some numerical differences between MDs and EMs for IEA15 MW blade case.
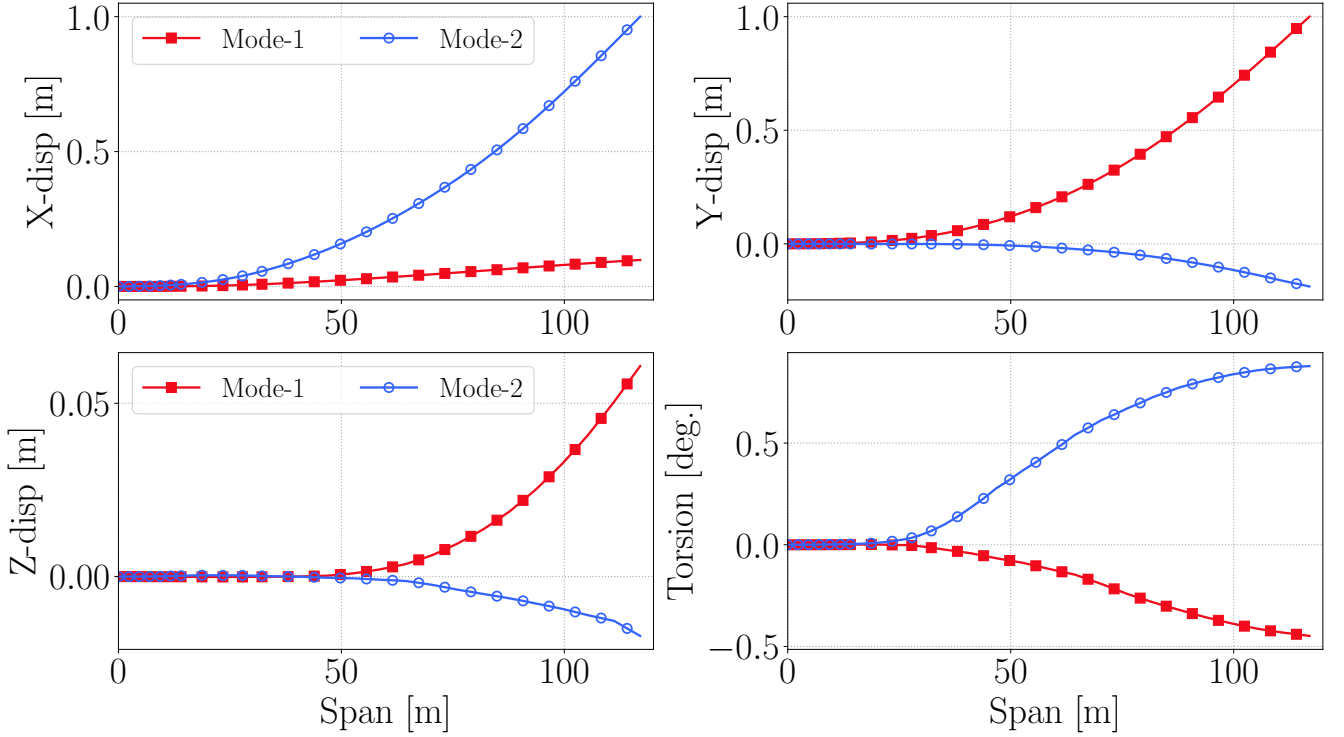
Figure 11. The lateral and torsional displacements of the first two mode shapes of IEA 15MW reference wind turbine blade.

The blade loads include aerodynamic loads at steady $11\,\mathrm{m\,s}^{-1}$ wind speed which gives the highest thrust force. The steady aerodynamic loads for symmetric rotor (no tilt, no yaw) is time independent (static) and their torsion components are not included for this example so that the torsion due to mode-shape couplings and dynamic forcing is more clear for this example. On top of the aerodynamic loads, the weight of the blade is applied in $x-$ (edgewise) direction with the formulation given in equation (18) where ω is $1.0\ rad/s$. There are 15 linear mode-shapes for blade ROM and quadratic vectors for first three modes are included only since these modes have very high modal amplitudes among all (see Table 5).

Figure 13 shows the tip displacement results of the blade in edgewise ($x-$), flapwise ($y-$), axial ($z-$) and torsion directions for linear ROM, HAWC2 and correction models. Since most of the thrust force is in flapwise direction, the largest displacements occur in that direction with mean displacement around $13.4\,\mathrm{m}$. The fluctuations in $y-$ direction is mostly due to couplings between mode-shapes, in other words it is mostly due to linear stiffness effects and not the nonlinear stiffness effects which is the case for straight beam example (see Figure 10 $x-$ direction results). Since nonlinear stiffness effects are very small in $x-$ and $y-$ displacements, the results are very similar in terms of magnitude and phase for all models.

The secondary effects become clear in $z-$ (axial) and torsion directions. The linear model has $0.84\,\mathrm{m}$ mean tip axial displacement for last $50\,\mathrm{s}$ due to mode-shape couplings (see Figure 11), however HAWC2 model has $-0.41\,\mathrm{m}$ mean tip axial displacements for the same time period. Hence, linear ROM estimates $2.5\,\mathrm{m}$ larger rotor diameter compared to HAWC2.
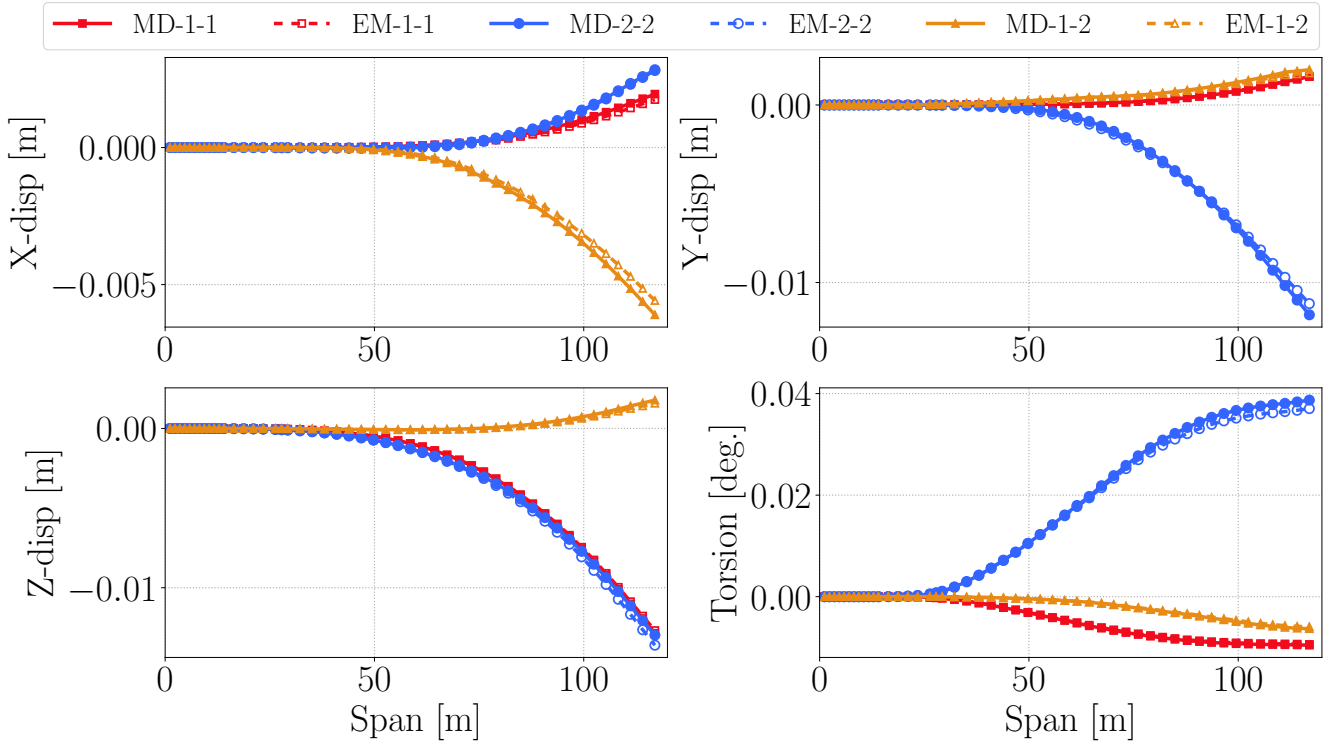
Figure 12. The first three modal derivatives and three expansion modes for the blade of the IEA 15MW reference wind turbine. The lines show the lateral and torsional displacements along the span of the blade length.

Table 5. IEA15MW blade mean modal amplitude results for last $50\,\mathrm{s}$ of the analysis

q_1	q_2	q_3	q_4	q_5	q_6	q_7
12.44	1.13	0.74	-0.17	0.23	0.28	0.34

Modal derivative correction model has $-0.29\,\mathrm{m}$ and expansion mode correction model has $-0.23\,\mathrm{m}$ mean axial ($z-$) displacements. They also represents the fluctuations in $z-$ directions much more accurately compared to the linear model which has almost no fluctuations for last $50\,\mathrm{s}$. Linear model maximum tip torsion error compared to HAWC2 for last $50\,\mathrm{s}$ is about $1.36°$. The maximum tip torsion error of MD and EM models for last $50\,\mathrm{s}$ are $0.63°$ and $0.26°$. The correction modes also capture

5 the phase of torsion motion more accurately than the linear model which is out of phase with HAWC2 in torsion direction. In this study, the load time series are prescribed and not updated with deflection. In other words, the results are not obtained for an aeroelastic analysis. On the other hand, the importance of torsion motion will increase for an aeroelastic analysis. The difference in mean torsion results are critical in static aeroelastic analysis where the steady operating conditions are determined. On the other hand, the difference in torsion fluctuations will affect the damage equivalent loads Gozcu and Verelst (2019) and

10 aeroelastic stability analysis Kallesøe (2011).
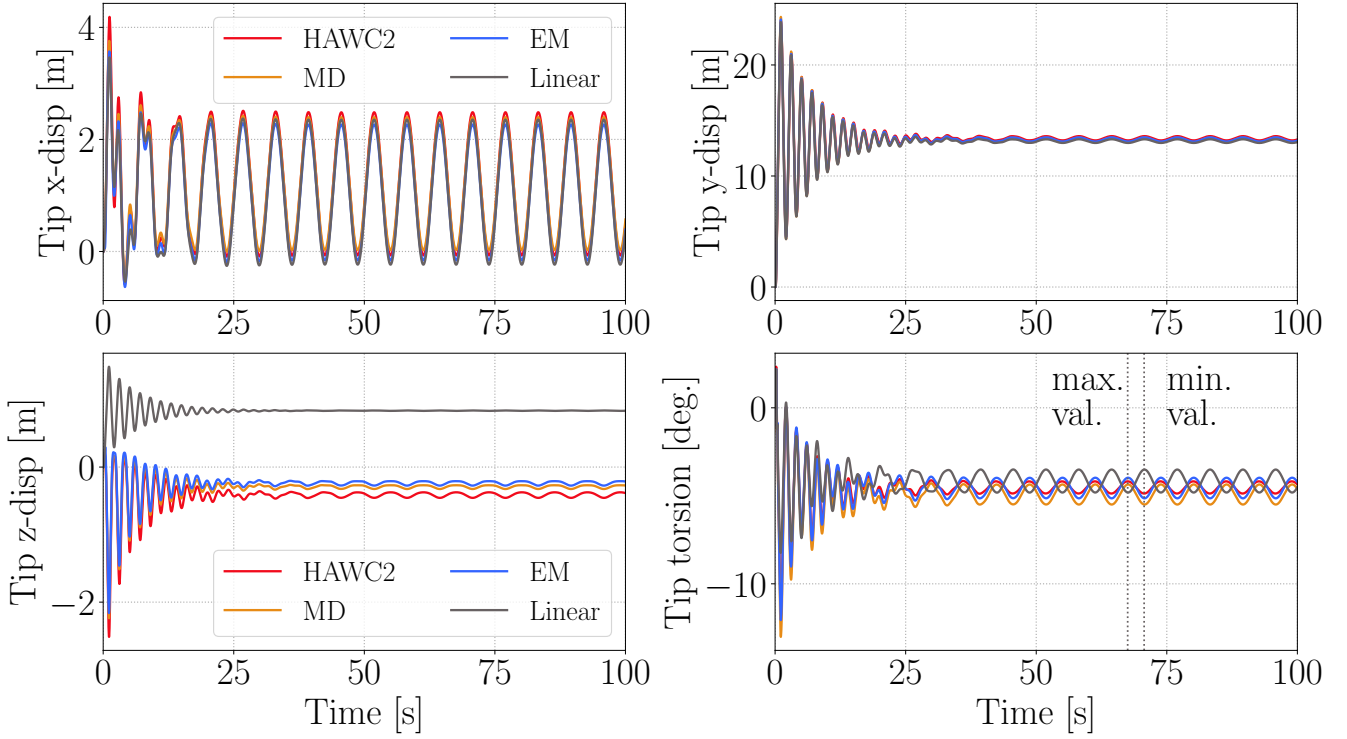
Figure 13. The lateral and torsional displacements for the blade tip of IEA 15MW wind turbine obtained by using HAWC2, linear ROM, MD correction, and EM correction.

Figure 14 and Figure 15 show the displacement results over the blade span at the two selected time steps where minimum and maximum torsion deflections are obtained in the last $50\,$s from HAWC2 (shown with black dashed lines). These time steps also correspond to maximum and minimum edgewise displacements. At $70.56\,$s where the maximum tip torsion occur, linear ROM results are quite accurate except $z-$ and $x-$ displacement (see Figure 14). On the other hand, MD and EM results are
5   much better than linear ROM results in all directions for that moment. Linear ROM has $1.29\,$m error in $z-$ direction at blade tip whereas MD and EM errors are less than $0.17\,$m for blade tip in figure 15. The linear ROM predicts a nonphysical elongation in the $z-$direction because of the non-zero motion in the $z-$direction in the linear mode shapes (particularly Mode-1) shown in Fig. 11. In contrast, the two correction methods in this study are not limited by the linear mode shapes. Both of the correction methods provide a correct estimation of the shortening of the blade in the axial direction.
10   Figure 14 shows displacement and torsion results along blade span at the maximum tip torsion moment ($67.51\,$s in Figure 13). Linear ROM is quite accurate in $x-$ and $y-$ direction, however it has low accuracy in $z-$ and torsion directions. Its total torsion error over the blade span is $33.6°$ whereas MD error is $7.7°$ and EM error is $1.7°$ along the blade span compared to HAWC2 results. The $z-$ direction results are similar to minimum torsion moment results in Figure 15.
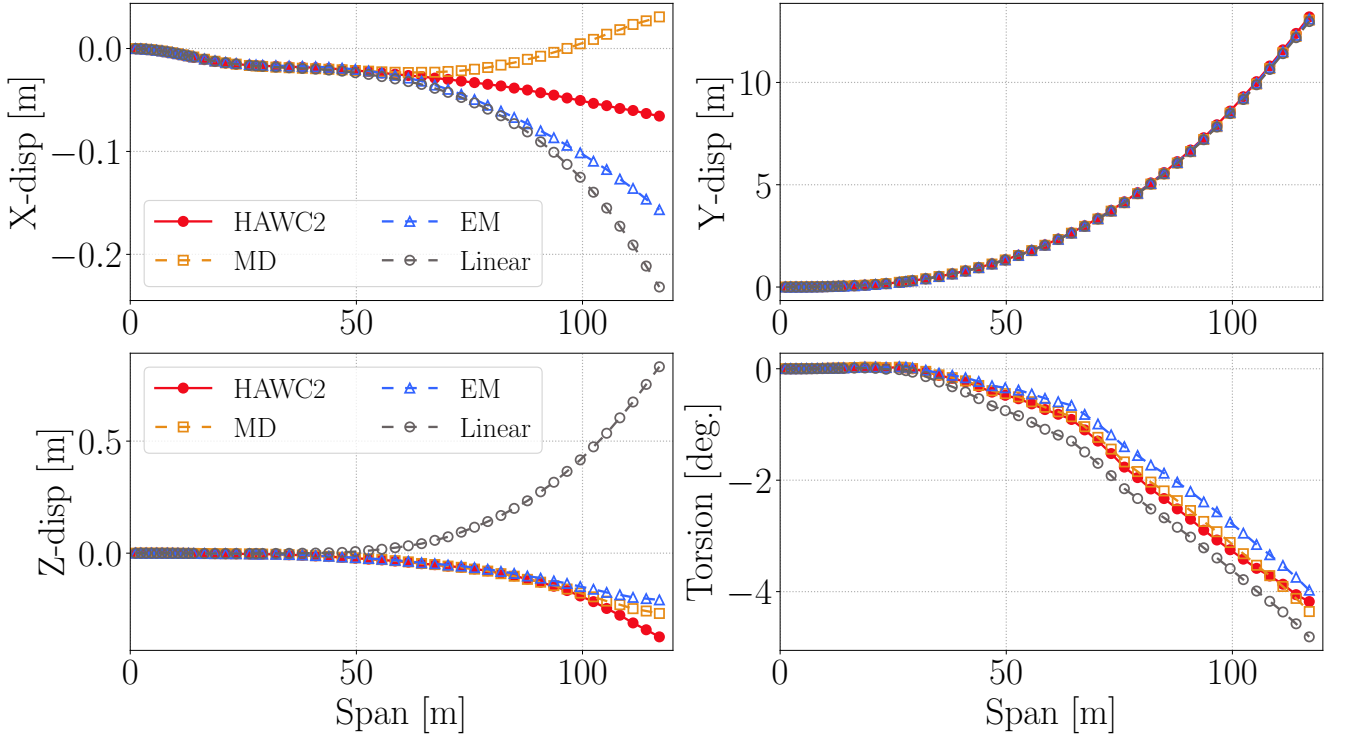
Figure 14. Spanwise deflection results at the time when the maximum torsion occurs (67.5 seconds)

One of the findings in Figure 10 and Figure 13 is that the frequency of the vibration is not affected by the large deflections of the blade. Even the linear model can predict the vibration frequency or the time period of the periodic response in good agreement with HAWC2 simulation in main deflection directions. In practice, this means that no correction is needed for the vibration frequency in case of large deflections. This also suits the application of the proposed correction method to a variety of slender cantilever structures including wind turbine blades. Besides, this allows using correction terms to capture secondary effects due to geometric nonlinearities for moderately large deflections.

5 Conclusions

This study introduced a correction approach for capturing the geometric nonlinear effects in the reduced order models of cantilever beam structures which go through the moderately large deflections. The approach is examined based on two different types of correction vectors (i.e. the modal derivatives and expansion modes) leading to similar results. Both correction vectors can be pre-computed by using a geometrically nonlinear beam solver, and then used in the dynamic response analysis. The advantage of this approach is its low computational cost during the coupled response analysis. It is suitable to be integrated
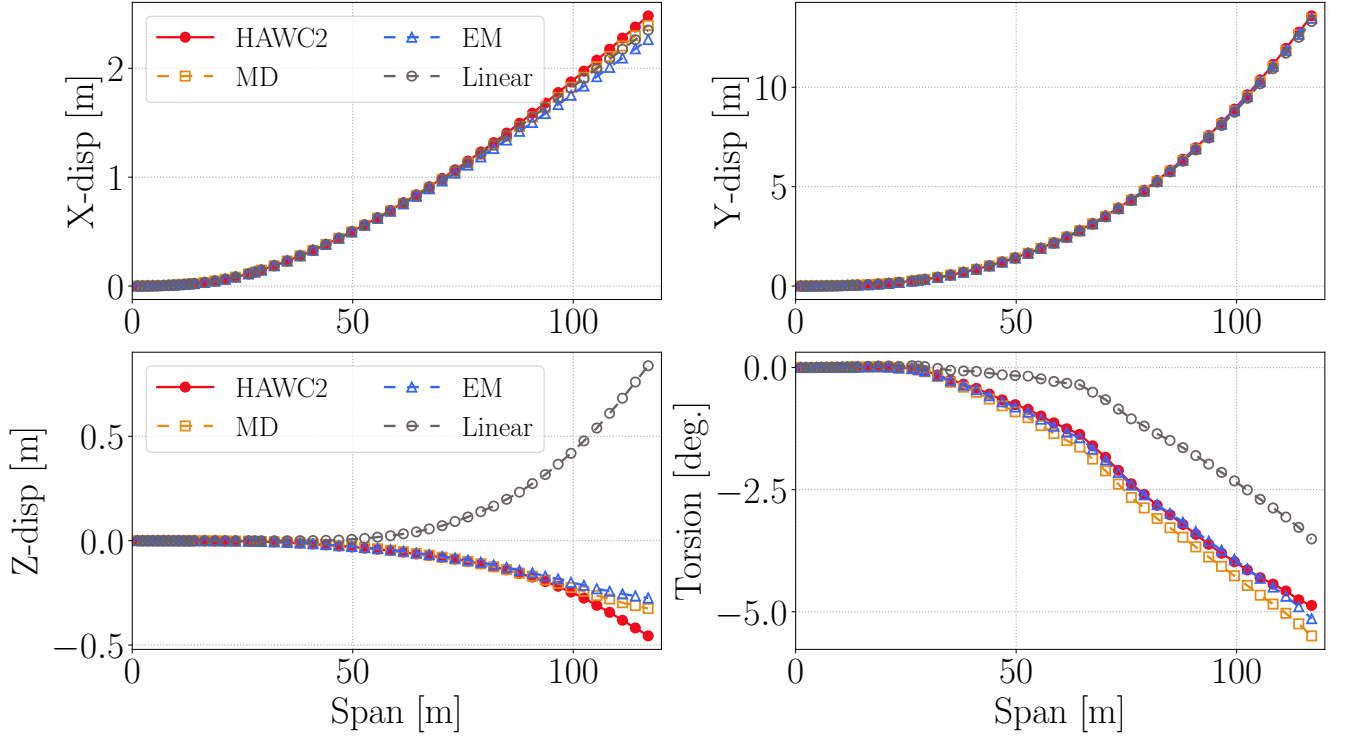
Figure 15. Spanwise deflection results at the time when the minimum torsion occurs (70.66 seconds)

into the aeroelastic analysis tools that use the modal based reduced order models for the cantilever beam structures such as wind turbine blades and airplane wings.

The proposed method is demonstrated by using two case studies, including a simple cantilever beam, and the blade for the IEA wind 15MW reference turbine. For the simple cantilever beam, its mode shapes are uncoupled in the sense that the displacements in the two bending modes are orthogonal two each other. For the turbine blade, its mode shapes are coupled because of its curved and twisted geometry and complex cross sectional properties. In the case study of the simple cantilever beam, the correction vectors based on the modal derivatives and expansion modes have identical results and they captured geometrically nonlinear effects accurately for the lateral deflections up to 25% of the beam length. In the case study of the blade of the IEA 15MW reference turbine, modal derivative and expansion mode vectors have small deviations from each other since they are computed by different numerical processes. The blade axial displacements estimated by the linear ROM are in opposite direction to the axial displacements in HAWC2 results. In other words, the linear ROM predicts a nonphysical elongation of IEA 15 MW blade span for the given load case. In contrast, the two correction vectors in this study give a good estimation of the axial motion of the blade tip. Further, the torsion displacements obtained by the linear ROM are out of phase with the HAWC2 results, whereas the torsion displacements obtained by using the two correction vectors in this study are in phase with the HAWC2 results. The torsion phase difference between nonlinear solver HAWC2 and linear ROM is crucial

for aeroelastic stability and load analysis of wind turbine blades. The comparison of these results shows that the proposed correction method is capable to accurately estimate the nonlinear dynamic response of the cantilever beam structures with large bending deflections, and it is also suitable for the wind turbine blades with curved and twisted geometry and complex cross sectional properties.

5   The study can be extended with an implementation of the correction method into an aeroelastic tool that uses the reduced order models for airplane wings or wind turbine blades. Further, the proposed correction method can also be implemented based on machine learning methods such as neural network models or adaptive kiriging methods.

Competing interests.   DTU Wind Energy develops, supports and distributes HAWC2 on commercial terms.

Acknowledgements.   The study was funded by DTU Wind and Orsted A.S.

References

Bauchau, O. A.: DYMORE user's manual: Formulation and finite element implementation of beam elements, University of Maryland, Maryland, 2009.

Beardsell, A., Collier, W., and Han, T.: Effect of linear and non-linear blade modelling techniques on simulated fatigue and extreme loads using Bladed, Journal of Physics: Conference Series, 753, 2016.

Bisplinghoff, R. L., Ashley, H., and Halfman, R. L.: Aeroelasticity, Courier Corporation, 2013.

Branlard, E. and Geisler, J.: A symbolic framework to obtain mid-fidelity models of flexible multibody systems with application to horizontal-axis wind turbines, Wind Energy Science, 7, 2351–2371, https://doi.org/10.5194/wes-7-2351-2022, https://wes.copernicus.org/articles/7/2351/2022/, 2022.

Branlard, E. S. P.: Flexible multibody dynamics using joint coordinates and the Rayleigh-Ritz approximation: The general framework behind and beyond Flex, Wind Energy, 22, 877–893, https://doi.org/10.1002/we.2327, https://onlinelibrary.wiley.com/doi/abs/10.1002/we.2327https://onlinelibrary.wiley.com/doi/10.1002/we.2327, 2019.

Cesnik, C. E., Palacios, R., and Reichenbach, E. Y.: Reexamined structural design procedures for very flexible aircraft, Journal of Aircraft, 51, 1580–1591, 2014.

Collier, W. and Sanz, J. M.: Comparison of linear and non-linear blade model predictions in Bladed to measurement data from GE 6MW wind turbine, in: Journal of Physics: Conference Series, vol. 753, p. 082004, IOP Publishing, 2016.

DNV: BLADED 4.8 Theory Manual, DNV GL, 2016.

Gaertner, E., Rinker, J., Sethuraman, L., Zahle, F., Anderson, B., Barter, G. E., Abbas, N. J., Meng, F., Bortolotti, P., Skrzypinski, W., et al.: IEA wind TCP task 37: definition of the IEA 15-megawatt offshore reference wind turbine, Tech. rep., National Renewable Energy Lab.(NREL), Golden, CO (United States), 2020.

Gozcu, O. and Verelst, D. R.: The effects of blade structural model fidelity on wind turbine load analysis and computation time, Wind Energy Science Discussions, 2019, 1–18, 2019.

Gözcü, O. and Dou, S.: Reduced order models for wind turbine blades with large deflections, Journal of Physics: Conference Series, 1618, 052 046, https://doi.org/10.1088/1742-6596/1618/5/052046, https://doi.org/10.1088/1742-6596/1618/5/052046, 2020.

Hansen, M.: Aerodynamics of wind turbines, Routledge, 2015.

Hollkamp, J. J. and Gordon, R. W.: Reduced-order models for nonlinear response prediction: Implicit condensation and expansion, Journal of Sound and Vibration, 318, 1139–1153, 2008.

Idelsohn, S. R. and Cardona, A.: A reduction method for nonlinear structural dynamic analysis, Computer Methods in Applied Mechanics and Engineering, 49, 253–279, 1985.

Jain, S., Tiso, P., Rutzmoser, J. B., and Rixen, D. J.: A quadratic manifold for model order reduction of nonlinear structural dynamics, Computers and Structures, 188, 80–94, 2017.

Jonkman, J. M. and Buhl Jr, M. L.: FAST User's Guide, National Renewable Energy Laboratory (NREL), 2005.

Kallesøe, B. S.: Effect of steady deflections on the aeroelastic stability of a turbine blade, Wind Energy, 14, 209–224, https://doi.org/10.1002/we.413, https://onlinelibrary.wiley.com/doi/10.1002/we.413, 2011.

Kim, K., Khanna, V., Wang, X., and Mignolet, M.: Nonlinear reduced order modeling of flat cantilevered structures, Proceedings of the 50th AIAA/ASME/ASCE/AHS/ASC Structures, Structural Dynamics, and Materials Conference, 2009.

Krenk, S.: Nonlinear Modelling and Analysis of Structures and Solids, Cambridge University Press, 2005.

Larsen, T. and Hansen, A.: How 2 HAWC2, the user's manual, Tech. Rep. R-1597 (ver. 12.8)(EN), DTU Wind Energy, 2019.

Marshall, M. and Pellegrino, S.: Reduced-Order Modeling for Flexible Spacecraft Deployment and Dynamics, in: AIAA Scitech 2021 Forum, p. 1385, 2021.

Pavese, C., Kim, T., Wang, Q., Jonkman, J., and Sprague, M. A.: Hawc2 and beamdyn: Comparison between beam structural models for
5   aero-servo-elastic frameworks, National Renewable Energy Lab.(NREL) Technical Report, 2016.

Riziotis, V., Voutsinas, S., Politis, E., Chaviaropoulos, P., Hansen, A. M., Madsen, A., and Rasmussen, F.: Identification of structural non-linearities due to large deflections on a 5 MW wind turbine blade, Proceedings of the EWEC, 8, 2008.

Rutzmoser, J. B., Rixen, D. J., Tiso, P., and Jain, S.: Generalization of quadratic manifolds for reduced order modeling of nonlinear structural dynamics, Computers and Structures, 192, 196–209, 2017.

10 Touzé, C., Vizzaccaro, A., and Thomas, O.: Model order reduction methods for geometrically nonlinear structures: a review of nonlinear techniques, Nonlinear Dynamics, 105, 1141–1190, https://doi.org/10.1007/s11071-021-06693-9, https://doi.org/10.1007/s11071-021-06693-9https://link.springer.com/10.1007/s11071-021-06693-9, 2021.

Wallrapp, O. and Schwertassek, R.: Representation of geometric stiffening in multibody system simulation, International Journal for Numerical Methods in Engineering, 32, 1833–1850, https://doi.org/https://doi.org/10.1002/nme.1620320818, https://onlinelibrary.wiley.com/doi/
15 abs/10.1002/nme.1620320818, 1991.

Wang, Q., Sprague, M. A., Jonkman, J., Johnson, N., and Jonkman, B.: BeamDyn: a high-fidelity wind turbine blade solver in the FAST modular framework, Wind Energy, 2017.

Wang, X., Perez, R. A., and Mignolet, M. P.: Nonlinear reduced order modeling of complex wing models, Proceedings of the 54th AIAA/ASME/ASCE/AHS/ASC Structures, Structural Dynamics, and Materials Conference, 2013.

20 Wu, L. and Tiso, P.: Modal Derivatives based Reduction Method for Finite Deflections in Floating Frame, Proceedings - WCCM XI: 11th World Congress on Computational Mechanics; ECCM V: 5th European Conference on Computational Mechanics; ECFD VI: 6th European Conference on Computational Fluid Dynamics, Barcelona, Spain, 20-25 July 2014, pp. 1–11, 2014.

Wu, L., Tiso, P., Tatsis, K., Chatzi, E., and van Keulen, F.: A modal derivatives enhanced Rubin substructuring method for geometrically nonlinear multibody systems, Multibody System Dynamics, pp. 57–85, 2018.